Inorg. Chem. **2008**, *47*, 1420−1427

Internal and External Factors in the Structural Organization in Cocrystals of the Mixed-Metal Endohedrals ($GdSc_2N@I_h$-C_{80}, $Gd_2ScN@I_h$-C_{80}, and $TbSc_2N@I_h$-C_{80}) and Nickel(II) Octaethylporphyrin

Steven Stevenson,[†] Christopher J. Chancellor,[‡] Hon Man Lee,[‡] Marilyn M. Olmstead,[‡] and Alan L. Balch*[,‡]

Department of Chemistry, University of California, Davis, One Shields Avenue, Davis, California 95616, and Department of Chemistry and Biochemistry, University of Southern Mississippi, Hattiesburg, Mississippi 39406

Received September 14, 2007

Structural characterizations of three new mixed-metal endohedrals, $GdSc_2N@I_h$-C_{80}, $Gd_2ScN@I_h$-C_{80}, and $TbSc_2@I_h$-C_{80}, have been obtained by single-crystal X-ray diffraction on $GdSc_2N@I_h$-C_{80}·Ni^{II}(OEP)·$2C_6H_6$, $Gd_2ScN@I_h$-C_{80}·Ni^{II}(OEP)·$2C_6H_6$, and $TbSc_2N@I_h$-C_{80}·Ni^{II}(OEP)·$2C_6H_6$. All three have I_h-C_{80} cages and planar MM'_2N units. The central nitride ion is positioned further from the larger Gd^{3+} or Tb^{3+} ions and closer to the smaller Sc^{3+} ions. The MM'_2N units show a remarkable degree of orientational order in these and related compounds in which the endohedral fullerene is cocrystallized with a metalloporphyrin. The MM'_2N units are oriented perpendicularly to the porphyrin plane and aligned along one of the N−Ni−N axes of the porphyrin. The smaller Sc^{3+} ions show a marked preference to lie near the porphyrin plane. The larger Gd^{3+} or Tb^{3+} ions assume positions further from the plane of the porphyrin. The roles of dipole forces and electrostatic forces in ordering these cocrystals of endohedral fullerenes and metalloporphyrins are considered.

Introduction

Endohedral fullerenes that consist of one or more metal atoms inside a closed cage of carbon atoms are generally prepared by the Krätschmer−Huffman arc vaporization of graphite and a suitable metal oxide in a low-pressure helium atmosphere.[1] Usually these endohedral fullerenes are produced in rather low yields. However, incorporation of a source of nitrogen into the arc process used for endohedral fullerene generation improves the yields of families of endohedrals in which M_3N units are encapsulated in various sizes of fullerene cages.[2–4] Of these products, $M_3N@C_{80}$ with an idealized I_h fullerene cage is particularly abundant, and significant improvements have been made in the separation and purification of this type of endohedral.[5,6]

Those endohedrals that contain paramagnetic metal ions hold promise for applications as relaxation agents for magnetic resonance imaging (MRI) and as components in nanomagnetic materials. For MRI applications, gadolinium complexes are particularly attractive because of the high magnetic moment of Gd^{3+}, which facilitates increases in the rate of relaxation for the protons of water. Consequently, chelated complexes of Gd^{3+} are widely utilized in biomedical MRI applications.[7,8] However, recent studies of water-soluble gadolinium endohedral fullerenes such as $Gd@C_{82}(OH)_n$, $Gd@C_{60}(OH)_x$, and $Gd@C_{60}[(C(COOH_yNa_{1-y})_2]_{10}$ have shown that these endohedrals have relaxivities up to 20 times greater

* To whom correspondence should be addressed. E-mail: albalch@ucdavis.edu.
† University of Southern Mississippi.
‡ University of California, Davis.

(1) Akasaka, T., Nagase, S. Eds. *Endofullerenes: A New Family of Carbon Clusters (Developments in Fullerene Science)*; Kluwer Academic Publishers: Dordrecht, The Netherlands, 2002.
(2) Stevenson, S.; Rice, G.; Glass, T.; Harich, K.; Cromer, F.; Jordan, M. R.; Craft, J.; Hadju, E.; Bible, R.; Olmstead, M. M.; Maitra, K.; Fisher, A. J.; Balch, A. L.; Dorn, H. C. *Nature* **1999**, *401*, 55.
(3) Zuo, T.; Beavers, C. M.; Duchamp, J. C.; Campbell, A.; Dorn, H. C.; Olmstead, M. M.; Balch, A. L. *J. Am. Chem. Soc.* **2007**, *129*, 2035.
(4) Yang, S.; Dunsch, L. *J. Phys. Chem. B* **2005**, *109*, 12320.
(5) Duchamp, J. C.; Cai, T.; Gibson, H. W.; Dorn, H. C. *J. Am. Chem. Soc.* **2005**, *127*, 16292.
(6) Stevenson, S.; Harich, K.; Yu, H.; Stephen, R. R.; Heaps, D.; Coumbe, C.; Phillips, J. P. *J. Am. Chem. Soc.* **2006**, *128*, 8829.
(7) Caravan, P.; Ellison, J. J.; McMurry, T. J.; Lauffer, R. B. *Chem. Rev.* **1999**, *99*, 2293.
(8) Bottrill, M.; Kwok, L.; Long, N. J. *Chem. Soc. Rev.* **2006**, *35*, 557.

10.1021/ic701824q CCC: $40.75
Published on Web 02/05/2008

than the conventional gadolinium chelates.[9–12] Moreover, the encapsulated gadolinium in an endohedral fullerene is more firmly bound than the gadolinium in currently utilized chelated complexes.

Endohedral fullerenes containing more than one paramagnetic metal ion may have additional advantages as relaxation agents because of the proximity of several paramagnetic centers in a confined space. Thus, we recently reported the preparation, separation, and structural isolation of $Gd_3N@I_h$-C_{80},[13–17] which has three paramagnetic Gd^{3+} ions and a nitride ion (N^{3-}) trapped in a $[C_{80}]^{6-}$ cage with I_h symmetry.[18] The Gd_3N unit in $Gd_3N@I_h$-C_{80} is pyramidal with the nitride ion 0.522(8) Å out of the plane of the three Gd^{3+} ions in the major orientation. Some of the physical and chemical properties of $Gd_3N@I_h$-C_{80} have also been reported,[19–21] and computational studies have examined the magnetic interactions between the gadolinium ions in $Gd_3N@I_h$-C_{80}.[22,23] The efficacy of $Gd_3N@I_h$-C_{80} as an MRI relaxation agent has been examined.[24]

Mixed-metal species of the types $MM'_2N@C_{80}$ and $MM'M''N@C_{80}$ can also be produced in the arc process of endohedral generation.[2,25,26] Of these mixed-metal endohedrals, $ErSc_2N@I_h$-C_{80}[27] and $CeSc_2N@I_h$-C_{80}[28] are particularly well characterized because both have been examined by single-crystal X-ray diffraction. Recently, the preparations and isolations of $GdSc_2N@C_{80}$ and $Gd_2ScN@C_{80}$ have also been reported.[29] On the basis of IR spectral data and density functional theory computations, Yang et al. proposed that the $GdSc_2N$ unit in $GdSc_2N@C_{80}$ would be planar while the Gd_2ScN unit in $Gd_2ScN@C_{80}$ would be pyramidal.[24] Here, we report crystallographic studies of $GdSc_2N@I_h$-C_{80}, $GdSc_2N@I_h$-C_{80}, and $TbSc_2@I_h$-C_{80}, which provide detailed structural characterization of these endohedrals and allow us to make comparisons among the structures of a complete family of endohedral fullerenes ($Sc_3N@I_h$-C_{80}, $GdSc_2N@I_h$-C_{80}, $Gd_2ScN@I_h$-C_{80}, and $Gd_3N@I_h$-C_{80}) in which the interior composition is systematically varied.

Results

Samples of $GdSc_2N@I_h$-C_{80}, $Gd_2ScN@I_h$-C_{80}, and $TbSc_2@I_h$-C_{80} were obtained utilizing procedures developed previously for the carbon arc method of preparation of endohedrals of the type $M_3N@C_{80}$.[2]

Structure of $GdSc_2N@I_h$-C_{80}·Ni^{II}(OEP)·$2C_6H_6$. Suitable crystals of this endohedral were obtained by diffusion of a benzene solution of Ni^{II}(OEP) into a solution of $GdSc_2N@I_h$-C_{80} in benzene over a 2-week period, and a similar procedure was used with the other endohedral fullerenes considered here. Black crystals with the composition $GdSc_2N@I_h$-C_{80}·Ni^{II}(OEP)·$2C_6H_6$ were obtained and characterized by X-ray diffraction. Crystal data are given in Table 1. Figure 1 shows a drawing of the endohedral and its relationship to the porphyrin. Both of these molecules reside in general positions and have no crystallographically imposed symmetry. Both the carbon cage, which has idealized I_h symmetry, and the $GdSc_2N$ unit inside are ordered. In addition, there are two molecules of benzene in general positions. Selected interatomic distances and angles for $GdSc_2N@I_h$-C_{80} and the other endohedrals considered here are collected in Table 2. Figure 2 shows the positioning of the metal atoms with respect to neighboring portions of the I_h-C_{80} cage.

(9) Mikawa, M.; Kato, H.; Okumura, M.; Narazaki, M.; Kanazawa, Y.; Miwa, N.; Shinohara, H. *Bioconjugate Chem.* **2001**, *12*, 510.

(10) Bolskar, R. D.; Benedetto, A. F.; Husebo, L. O.; Price, R. E.; Jackson, E. F.; Wallace, S.; Wilson, L. J.; Alford, J. M. *J. Am. Chem. Soc.* **2003**, *125*, 5471.

(11) Tóth, E.; Bolskar, R. D.; Borel, A.; González, G.; Helm, L.; Merbach, A. E.; Sitharaman, B.; Wilson, L. J. *J. Am. Chem. Soc.* **2005**, *127*, 799.

(12) Miyamoto, A.; Okimoto, H.; Shinohara, H.; Shibamoto, Y. *Eur. Radiol.* **2006**, *16*, 1050.

(13) In response to a cogent reviewer's comments, we have adopted the following nomenclature in discussing these endohedrals. The symbol $Sc_3N@I_h$-C_{80} is used to indicate that the Sc_3N unit resides inside a fullerene cage with *idealized* I_h symmetry. Such a symbolism is needed because endohedrals are known to exist with various cage isomers; e.g., both $Sc_3N@I_h$-C_{80} and $Sc_3N@D_{5h}$-C_{80} have been isolated, purified, and crystallographically characterized.[15] Thus, it is important to specify which specific cage isomer is involved once that information has been ascertained. In cases where there is more than one cage isomer with a particular cage symmetry, further identification can be specified by adding, in parentheses, the number of that isomer from the list given by Fowler and Manolopoulos.[14] For example, there are five isomers of C_{78} that obey the isolated pentagon rule (IPR), with each of their 12 pentagons surrounded by 5 hexagons: two with D_{3h} symmetry, two with C_{2v} symmetry, and one with D_3 symmetry. Thus, for endohedrals utilizing a 78-carbon-atom cage, it is necessary to specify which specific D_{3h} or C_{2v} isomer is present. We will use the symbol $Sc_3N@D_{3h}(5)$-C_{78} to identify this crystallographically characterized molecule.[16] For endohedrals that do not obey the IPR, the number of possible cage isomers can be quite large. Thus, the symbol $Tb_3N@C_s(51365)$-C_{84} identifies the crystallographically characterized isomer of this endohedral as isomer 51 365 with C_s symmetry from a compilation of 51 568 non-IPR isomers of the C_{84} cage.[17] It is important to note that the symmetry designations used here refer to the idealized symmetry of the cage only. In general, the overall symmetry of the entire endohedral will be lower than that of the cage individually because of the placement of the atoms on the inside.

(14) Fowler, P. W.; Manolopoulos, D. E. *An Atlas of Fullerenes*; Clarendon Press: Oxford, U.K., 1995.

(15) Cai, T.; Xu, L.; Anderson, M. R.; Ge, Z.; Zuo, T.; Wang, X.; Olmstead, M. M.; Balch, A. L.; Gibson Dorn, H. C. *J. Am. Chem. Soc.* **2006**, *128*, 8581.

(16) Olmstead, M. M.; de Bettencourt-Dias, A.; Duchamp, J. C.; Stevenson, S.; Marciu, D.; Dorn, H. C.; Balch, A. L. *Angew. Chem., Int. Ed.* **2001**, *40*, 1223.

(17) Beavers, C. M.; Zuo, T.; Duchamp, J. C.; Harich, K.; Dorn, H. C.; Olmstead, M. M.; Balch, A. L. *J. Am. Chem. Soc.* **2006**, *128*, 11352.

(18) Stevenson, S.; Phillips, J. P.; Reid, J. E.; Olmstead, M. M.; Rath, S. P.; Balch, A. L. *Chem. Commun.* **2004**, 2814.

(19) Krause, M.; Dunsch, L. *Angew. Chem., Int. Ed.* **2005**, *44*, 1557.

(20) Stevenson, S.; Stephen, R. R.; Amos, T. M.; Cadorette, V. R.; Reid, J. E.; Phillips, J. P. *J. Am. Chem. Soc.* **2005**, *127*, 12776.

(21) Chen, N.; Zhang, E. Y.; Tan, K.; Wang, C. R.; Lu, X. *Org. Lett.* **2007**, *9*, 2011.

(22) Lu, J.; Sabirianov, R. F.; Mei, W. N.; Gao, Y.; Duan, C. G.; Zeng, X. C. *J. Phys. Chem. B* **2006**, *110*, 23637.

(23) Qian, M. C.; Ong, S. V.; Khanna, S. N.; Knickelbein, M. B. *Phys. Rev. B* **2007**, *75*, 104424.

(24) Fatouros, P. P.; Corwin, F. D.; Chen, Z. J.; Broaddus, W. C.; Tatum, J. L.; Kettenmann, B.; Ge, Z.; Gibson, H. W.; Russ, J. L.; Leonard, A. P.; Duchamp, J. C.; Dorn, H. C. *Radiology* **2006**, *240*, 756.

(25) Dorn, H. C.; Iezzi, E. B.; Stevenson, S.; Balch, A. L.; Dunchamp, J. C. In *Endofullerenes*; Akasaka, T., Nagase, S., Eds.; Kluwer Academic Publishers: Dordrecht, The Netherlands, 2002; p 121.

(26) Chen, N.; Zhang, E. Y.; Wang, C. R. *J. Phys. Chem. B* **2006**, *110*, 13322.

(27) Olmstead, M. M.; de Bettencourt-Dias, A.; Duchamp, J. C.; Stevenson, S.; Dorn, H. C.; Balch, A. L *J. Am. Chem. Soc.* **2000**, *122*, 12220.

(28) Wang, X.; Zuo, T.; Olmstead, M. M.; Duchamp, J. C.; Glass, T. E.; Cromer, T. E.; Balch, A. L.; Dorn, H. C. *J. Am. Chem. Soc.* **2006**, *128*, 8884.

(29) Yang, S.; Kalbac, M.; Popov, A.; Dunsch, L. *ChemPhysChem* **2006**, *7*, 1990.

Table 1. Crystallographic Data[a]

	$GdSc_2N@I_h$-C_{80}·Ni^{II}(OEP)·$2C_6H_6$	$Gd_2ScN@I_h$-C_{80}·Ni^{II}(OEP)·$2C_6H_6$	$TbSc_2N@I_h$-C_{80}·Ni^{II}(OEP)·$2C_6H_6$
color/habit	black parallelepiped	black parallelepiped	black parallelepiped
formula	$C_{128}H_{56}GdN_5NiSc_2$	$C_{128}H_{56}Gd_2N_5NiSc$	$C_{128}H_{56}N_5NiSc_2Tb$
fw	1969.66	2081.95	1971.33
cryst syst	monoclinic	monoclinic	monoclinic
space group	*C*2/*c*	*I*2/*a*	*C*2/*m*
a, Å	25.074(5)	25.3061(11)	25.180(2)
b, Å	14.916(3)	15.0474(7)	15.0633(13)
c, Å	39.354(8)	39.377(2)	19.650(2)
α, deg	90	90	90
β, deg	94.99(3)	95.2160(10)	94.791(2)
γ, deg	90	90	90
V, Å^3	14663(5)	14932.2(13)	7427.1(12)
Z	8	8	4
T, K	100(2)	90(2)	100(2)
λ, Å	0.751 00	0.710 73	0.751 00
D, g/cm^3	1.784	1.852	1.763
μ, mm^{-1}	1.396	2.161	1.438
R1 (obsd data)	0.090	0.033	0.086
wR2 (all data)	0.277	0.077	0.230

[a] For data with $I > 2I$, $R1 = \sum||F_o| - |F_c|| / \sum|F_o|$. For all data, $wR2 = \sqrt{\sum[w(F_o^2 - F_c^2)^2] / \sum[w(F_o^2)^2]}$.

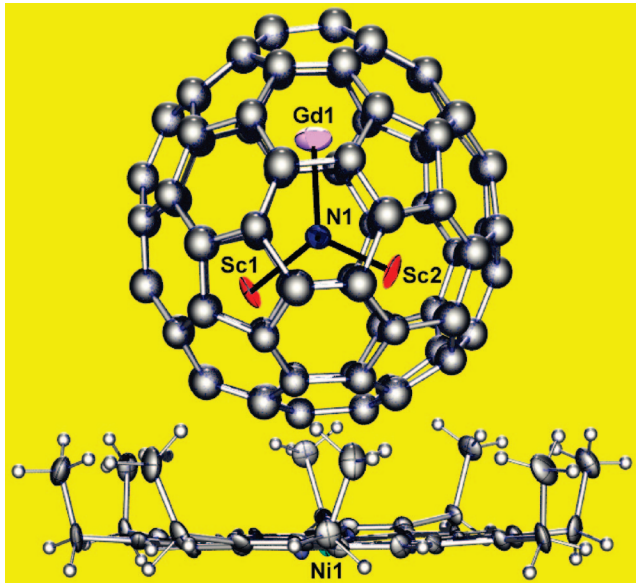

Figure 1. Perspective view of the relative orientations of $GdSc_2N@I_h$-C_{80} and Ni^{II}(OEP) within crystalline $GdSc_2N@I_h$-C_{80}·Ni^{II}(OEP)·$2C_6H_6$. Thermal ellipsoids are shown at the 50% probability level.

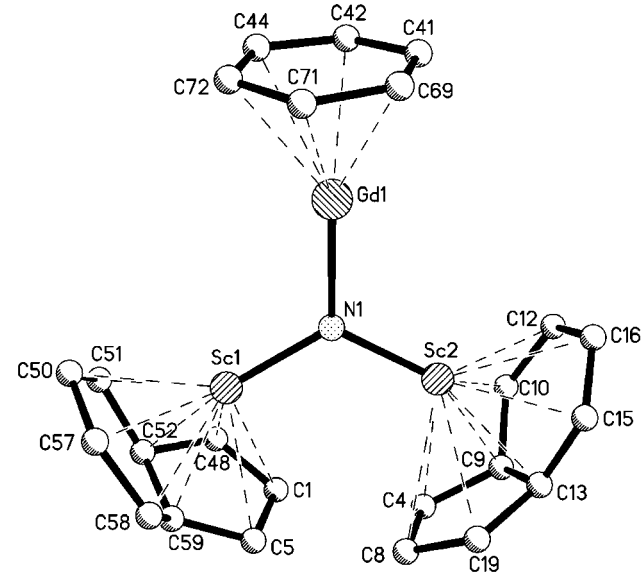

Figure 2. Positions of the nearest carbon atoms of the I_h-C_{80} cage and the $GdSc_2N$ unit in $GdSc_2N@I_h$-C_{80}·Ni^{II}(OEP)·$2C_6H_6$. The Gd−C distances in the nearest six-membered ring range from 2.459(14) Å for Gd1−C71 to 2.509(14) Å for Gd1−C42. The shortest Sc−C distances are Sc1−C59 = 2.268(14) Å and Sc1−C52 = 2.236(13) Å for Sc1 and Sc2−C9 = 2.267(12) Å and Sc2−C15 = 2.381(13) Å for Sc2.

Structure of $Gd_2ScN@I_h$-C_{80}·Ni^{II}(OEP)·$2C_6H_6$. Figure 3shows a drawing that demonstrates how the endohedral is nestled into a face of the porphyrin. While the C_{80} cage with idealized I_h symmetry is ordered, the endohedral molecule contains disordered gadolinium and scandium atoms that can be assigned to two sets of positions for the Gd_2ScN unit. Both involve a common nitrogen atom. The two sets of two gadolinium atoms and one scandium atom, {Gd1, Gd2, Sc1} and {Gd3, Gd4, Sc2}, refined to set occupancies of 0.851(5) and 0.149(5), respectively. Each gadolinium and scandium atom was allowed to refine separately with anisotropic thermal parameters. Only the predominant set {Gd1, Gd2, Sc1} is shown in Figure 3. The distances given in Table 2 also refer to the predominant set {Gd1, Gd2, Sc1}. The positioning of the metal atoms within the C_{80} cage is shown in Figure 4 for the predominant set of metal ion positions. While several endohedrals of the $MSc_2N@I_h$-C_{80} class have been crystallogaphically characterized, this compound represents the first example of an endohedral of the type $M_2ScN@I_h$-C_{80} to be characterized by X-ray diffraction.

Structure of $TbSc_2N@I_h$-C_{80}·Ni^{II}(OEP)·$2C_6H_6$. Figure 5 shows a drawing of the crystallographically determined structure. The Ni^{II}(OEP) molecule resides on a crystallographic mirror plane that bisects the nickel atom, N2, and N4. There are two orientations of the I_h-C_{80} cage that occupy a common site, which is bisected by a crystallographic mirror plane. That mirror plane does not coincide with a mirror plane of the I_h-C_{80} cage. Hence, the asymmetric unit consists of halves of the C_{80} cage, with the remaining parts generated by the mirror plane. Only one orientation of the C_{80} cage is shown in Figure 5. The $TbSc_2N$ unit is also disordered. The major set, with 0.60 occupancy, is comprised of Tb1 (with 0.38 fractional occupancy), Sc1 (with 0.60 fractional occupancy), and the

Table 2. Selected Interatomic Distances and Angles

	$Sc_3N@I_h$-C_{80}•5*o*-xylene[a]	$GdSc_2N@I_h$-C_{80}•Ni^{II}(OEP)•$2C_6H_6$	$Gd_2ScN@I_h$-C_{80}•Ni^{II}(OEP)•$2C_6H_6$	$Gd_3N@I_h$-C_{80}•Ni^{II}(OEP)•$1.5C_6H_6$[b]	$TbSc_2N@I_h$-C_{80}•Ni^{II}(OEP)•$2C_6H_6$
			Distances (Å)		
M−N	1.9931(14) Sc1	1.916(9) Sc1	1.911(3) Sc1	2.038(8) Gd1	1.949(8) Sc1
M−N	2.0323(16) Sc2	1.919(8) Sc1	2.072(3) Gd1	2.085(4) Gd2	1.949(8) Sc1#1
M−N	2.0526(14) Sc3	2.149(10) Gd	2.102(3) Gd2	2.117(5) Gd3	2.126(11) Tb1
			Three Shortest		
M−C	2.205(4) Sc1 2.219(4) 2.498(4)	2.236(13) Sc1 2.268(13) 2.302(13)	2.246(4) Sc1 2.269(4) 2.349(4)	2.344(13) Gd1 2.403(12) 2.483(10)	2.138(7) Sc1 2.237(7) 2.266(7)
M−C	2.145(4) Sc2 2.204(4) 2.367(4)	2.267(12) Sc2 2.278(13) 2.381(13)	2.456(4) Gd1 2.462(4) 2.467(4)	2.402(10) Gd2 2.415(11) 2.454(11)	2.190(6) Sc1 2.312(7) 2.350(7)
M−C	2.147(4) Sc3 2.255(4) 2.302(4)	2.459(14) Gd 2.469(14) 2.480(14)	2.394(4) Gd2 2.435(4) 2.450(4)	2.439(12) Gd3 2.440(11) 2.442(11)	2.416(3) Tb 2.442(5) 2.463(5)
			Angles (deg)		
M−N−M	120.70(7) Sc1−N−Sc2	118.3(5) Sc1−N1−Sc2	117.31(15) Sc1−N1−Gd1	111.6(2) Gd1−N1a−Gd2	129.0(4) Sc1−N−Tb1
M−N−M	119.21(6) Sc2−N−Sc3	121.7(4) Sc1−N1−Gd	123.81(16) Sc1−N1−Gd2	119.7(3) Gd1−N1a−Gd3	116.0(4) Sc1#1−N− Tb1
M−N−M	118.47(7) Sc1−N−Sc3	120.1(4) Sc2−N1−Gd	118.82(14) Gd1−N1−Gd2	110.3(3) Gd2−N1a−Gd3	115.0(7) Sc1−N−Sc1#1
Σ(M−N−M)	358.38	360.1	359.94	341.6	360.0

[a] Data from: Stevenson, S.; Lee, H. M.; Olmstead, M. M.; Kozikowski, C.; Stevenson, P.; Balch, A. L. *Chem.—Eur. J.* **2002**, *8*, 4528. [b] Data from: Stevenson, S.; Phillips, J. P.; Reid, J. E.; Olmstead, M. M.; Rath, S. P.; Balch, A. L. *Chem. Commun.* **2004**, 2814.

Figure 3. Perspective view of the relative orientations of $Gd_2ScN@I_h$-C_{80} and Ni^{II}(OEP) within crystalline $Gd_2ScN@I_h$-C_{80}•Ni^{II}(OEP)•$2C_6H_6$. Thermal ellipsoids are shown at the 50% probability level. The predominant set {Gd1, Gd2, Sc1} of metal ion positions with an occupancy of 0.851(5) is shown.

Figure 4. Position of the nearest carbon atoms of the I_h-C_{80} cage and the predominant Gd_2ScN unit in $Gd_2ScN@I_h$-C_{80}•Ni^{II}(OEP)•$2C_6H_6$. The Gd−C distances in the nearest six-membered ring range from 2.456(4) Å (Gd1−C55) to 2.486(4) Å (Gd1−C57) for Gd1 and from 2.394(4) Å (Gd2−C65) to 2.641(4) Å (Gd2−C77) for Gd2. The shortest Sc−C distances are Sc1−C4 = 2.246(4) Å and Sc1−C3 = 2.269(4) Å.

latter's mirror image. There are two other terbium atom sites: Tb1B, which resides on the crystallographic mirror plane with 0.10 fractional occupancy, and Tb1C in a general position with 0.07 fractional occupancy. Additionally, there are two other scandium atom sites, Sc1B and Sc1C, in general positions with 0.20 fractional occupancy for each. Figure 6 shows the relationship between the location of the major set of $TbSc_2$ positions and the

(30) Campanera, J. M.; Bo, C.; Olmstead, M. M.; Balch, A. L.; Poblet, J. M. *J. Phys. Chem. A* **2002**, *106*, 12356.

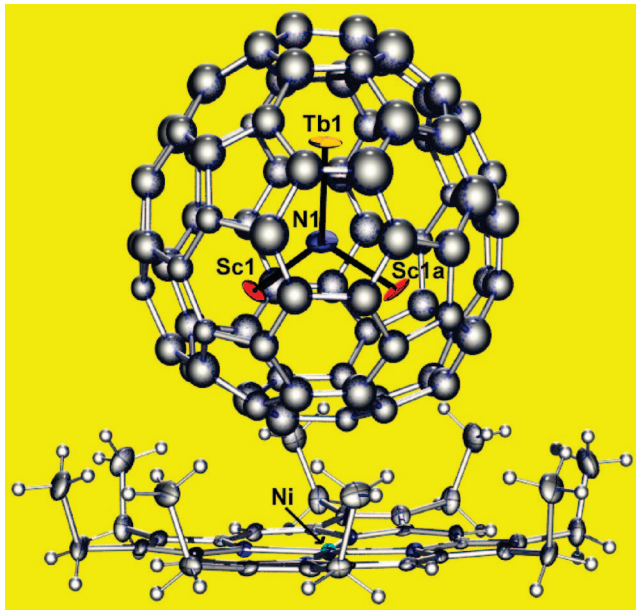

Figure 5. Perspective view of the relative orientations of $TbSc_2N@I_h$-C_{80} and Ni^{II}(OEP) within crystalline $TbSc_2N@I_h$-C_{80}·Ni^{II}(OEP)·$2C_6H_6$. Thermal ellipsoids are shown at the 50% probability level.

neighboring carbon atoms of the I_h-C_{80} cage.

Discussion

The results reported here demonstrate the ability of cocrystallization with Ni^{II}(OEP) to produce remarkably well-ordered crystals of the I_h-C_{80} endohedrals, even in situations where there are two different types of metal ions inside the cage and there is the option for considerable disorder. Computational studies have shown that scandium ions are not trapped in a specific position inside the carbon cage of $Sc_3N@I_h$-C_{80}.[30] Thus, the Sc_3 group is likely to rotate rather freely within $Sc_3N@I_h$-C_{80}, a situation that is consistent with the observation that the ^{13}C NMR spectrum of $Sc_3N@I_h$-C_{80} shows only two resonances in solution at room temperature.[2] The low barrier to movement of the Sc_3 group in $Sc_3N@I_h$-C_{80} is also consistent with the crystallographic data obtained from $Sc_3N@I_h$-C_{80}·5*o*-xylene and $Lu_3N@I_h$-C_{80}·5*o*-xylene, which show multiple positions for the metal ions inside the cage.[31] Of course, it may be that larger metal ions like Gd^{3+} and Tb^{3+} have a greater barrier to mobility within the idealized I_h C_{80} cage. Further computations to examine the mobility of larger, heavier metal ions in these cages could be enlightening.

The MM'_2N units in all three mixed-metal endohedrals studied here are planar. Relevant data are given in Table 2. Figure 7 shows edge-on views of the $M_nSc_{3-n}N$ units in $Sc_3N@I_h$-C_{80}, $GdSc_2N@I_h$-C_{80}, and $Gd_2ScN@I_h$-C_{80}. Thus, in the series $Sc_3N@I_h$-C_{80}, $GdSc_2N@I_h$-C_{80}, $Gd_2ScN@I_h$-C_{80}, and $Gd_3N@I_h$-C_{80}, only $Gd_3N@I_h$-C_{80} has a pyramidalized Gd_3N core. Yang et al. were correct to surmise that $GdSc_2N@I_h$-C_{80} has a planar core, but they were unable to ascertain the planar structure for $Gd_2ScN@I_h$-C_{80}.[24] As noted previously,[13] the pyramidalization of $Gd_3N@I_h$-C_{80} results

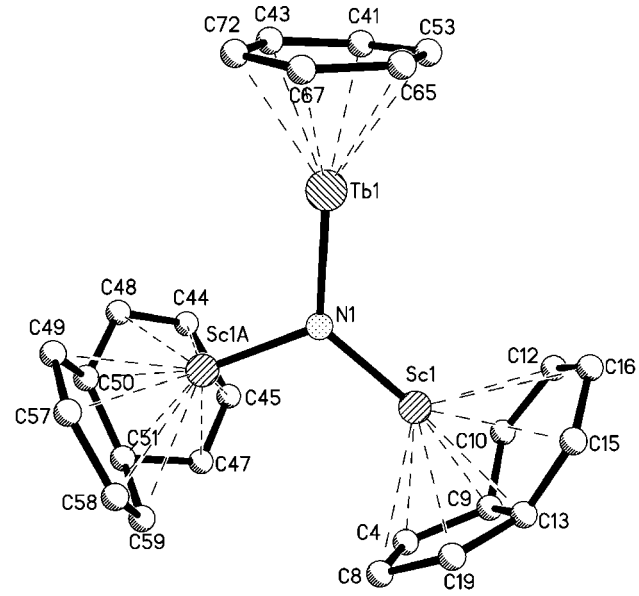

Figure 6. Position of the nearest carbon atoms of the I_h-C_{80} cage and the major set of $TbSc_2N$ sites (0.60 occupancy) in $TbSc_2N@I_h$-C_{80}·Ni^{II}(OEP)·$2C_6H_6$. The Tb−C distances in the nearest six-membered ring range from 2.416(3) Å (Tb−C67) to 2.507(3) Å (Tb−C41). The shortest Sc−C distances for Sc1 are 2.190(6) Å (Sc1−C9) and 2.312(7) Å (Sc1−C13), and for Sc1A, they are 2.138(7) Å (Sc1A−C50) and 2.237(7) Å (Sc1A−C51).

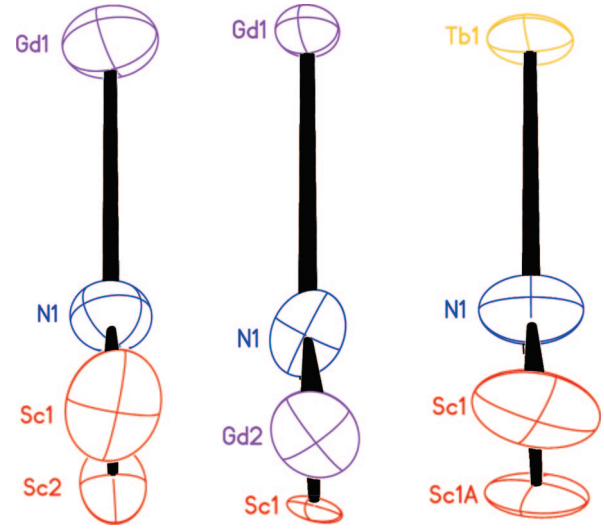

Figure 7. Edge-on views of the $M_nSc_{3-n}N$ units in $GdSc_2N@I_h$-C_{80}·Ni^{II}(OEP)·$2C_6H_6$, $Gd_2ScN@I_h$-C_{80}·Ni^{II}(OEP)·$2C_6H_6$, and $TbSc_2N@I_h$-C_{80}·Ni^{II}(OEP)·$2C_6H_6$. Thermal ellipsoids are shown at the 50% probability level.

from the need to accommodate three rather large Gd^{3+} ions within the C_{80} cage. The ionic radius for Gd^{3+} is 1.08 Å, and for Tb^{3+}, it is 1.06 Å, whereas the ionic radius for Sc^{3+} is only 0.88 Å.[32] Thus, the smaller size of the Sc^{3+} ion allows the necessary bond shortening to accommodate planar cores for $Sc_3N@I_h$-C_{80}, $GdSc_2N@I_h$-C_{80}, $Gd_2ScN@I_h$-C_{80}, and $GdSc_2N@I_h$-C_{80}. The consequences of the differences in the sizes of the two ions are seen in the data in Table 2. As the data show, the Sc−N distances are longest in $Sc_3N@I_h$-C_{80} and shorten progressively in the series $Sc_3N@I_h$-C_{80}, $GdSc_2N@I_h$-

(31) Stevenson, S.; Lee, H. M.; Olmstead, M. M.; Kozikowski, C.; Stevenson, P.; Balch, A. L. *Chem.—Eur. J.* **2002**, *8*, 4528.

(32) Shannon, R. D. *Acta Crystallogr.* **1976**, *A32*, 751.

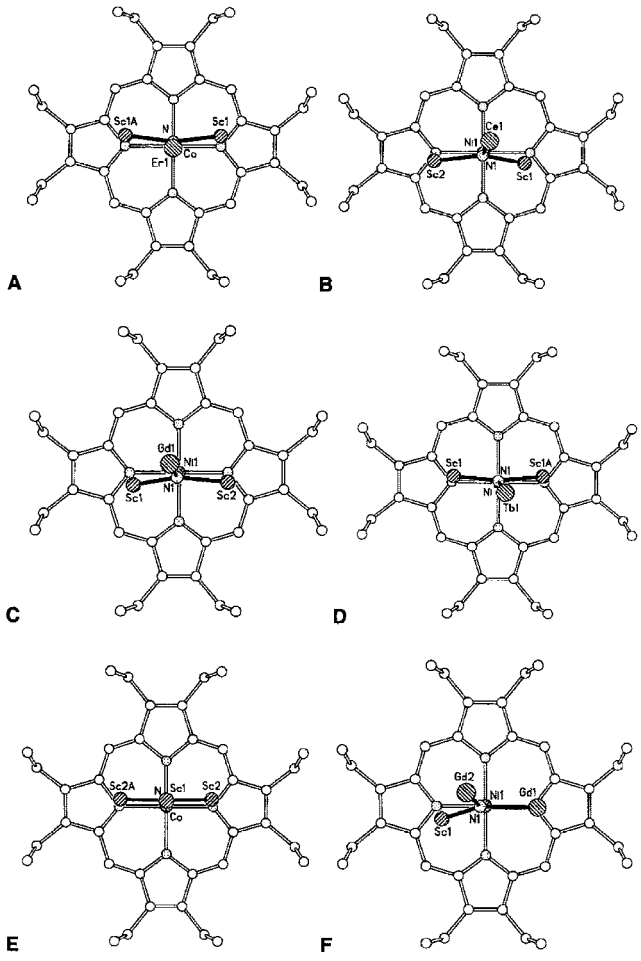

Figure 8. Views of the M_3N units from a vantage point perpendicular to the plane of the metalloporphyrin for (A) $ErSc_2N@I_h$-C_{80}•$1.5C_6H_6$•$0.3CH_6Cl_3$ (from Olmstead, M. M.; de Bettencourt-Dias, A.; Duchamp, J. C.; Stevenson, S.; Dorn, H. C.; Balch, A. L. *J. Am. Chem. Soc.* **2000**, *122*, 12220), (B) $CeSc_2N@I_h$-C_{80}•Ni^{II}(OEP)•$2C_6H_6$ (from Wang, X.; Zuo, T.; Olmstead, M. M.; Duchamp, J. C.; Glass, T. E.; Cromer, T. E.; Balch, A. L.; Dorn, H. C. *J. Am. Chem. Soc.* **2006**, *128*, 8884), (C) $GdSc_2N@I_h$-C_{80}•Ni^{II}(OEP)•$2C_6H_6$ (this work), (D) $TbSc_2N@I_h$-C_{80}•Ni^{II}(OEP)•$2C_6H_6$ (this work), (E) $Sc_3N@I_h$-C_{80}•Co^{II}(OEP)•$CHCl_3$•$0.5C_6H_6$ (from Stevenson, S.; Rice, G.; Glass, T.; Harich, K.; Cromer, F.; Jordan, M. R.; Craft, J.; Hadju, E.; Bible, R.; Olmstead, M. M.; Maitra, K.; Fisher, A. J.; Balch, A. L.; Dorn, H. C. *Nature* **1999**, *401*, 55), and (F) $Gd_2ScN@I_h$-C_{80}•Ni^{II}(OEP)•$2C_6H_6$ (this work). The I_h-C_{80} cage has been omitted from these drawings for clarity.

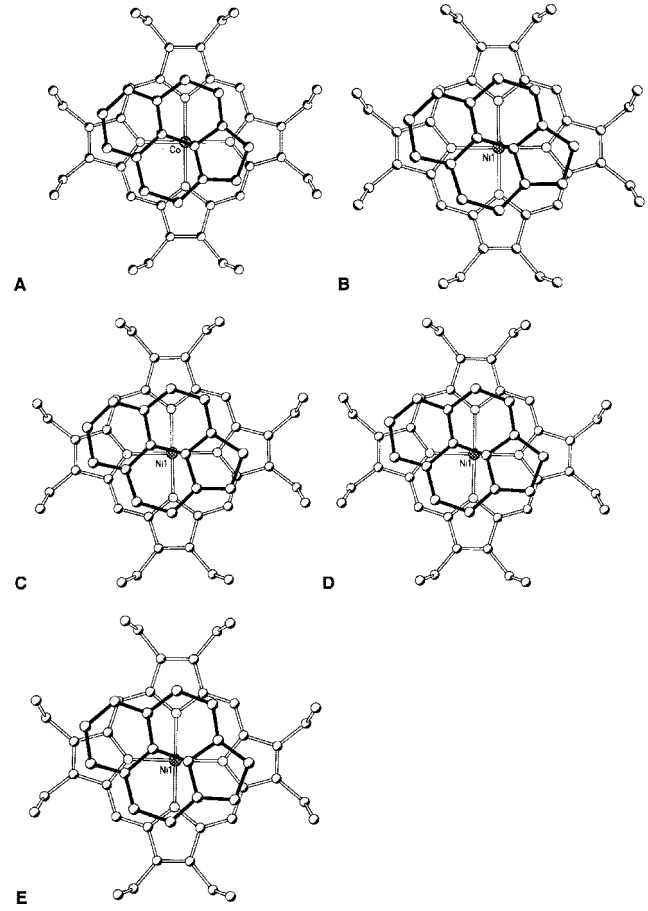

Figure 9. Views of a portion of the I_h-C_{80} cage (shown with solid lines) from a vantage point perpendicular to the plane of the metalloporphyrin (shown with hollow lines) for (A) $ErSc_2N@I_h$-C_{80}•$1.5C_6H_6$•$0.3CH_6Cl_3$ (from Olmstead, M. M.; de Bettencourt-Dias, A.; Duchamp, J. C.; Stevenson, S.; Dorn, H. C.; Balch, A. L. *J. Am. Chem. Soc.* **2000**, *122*, 12220), (B) $CeSc_2N@I_h$-C_{80}•Ni^{II}(OEP)•$2C_6H_6$ (from Wang, X.; Zuo, T.; Olmstead, M. M.; Duchamp, J. C.; Glass, T. E.; Cromer, T. E.; Balch, A. L.; Dorn, H. C. *J. Am. Chem. Soc.* **2006**, *128*, 8884), (C) $GdSc_2N@I_h$-C_{80}•Ni^{II}(OEP)•$2C_6H_6$ (this work), (D) $TbSc_2N@I_h$-C_{80}•Ni^{II}(OEP)•$2C_6H_6$ (this work), and (E) $Gd_2ScN@I_h$-C_{80}•Ni^{II}(OEP)•$2C_6H_6$ (this work).

C_{80}, and $Gd_2ScN@I_h$-C_{80}. Likewise, the Gd−N distances in $GdSc_2N@I_h$-C_{80} are longer than they are in $Gd_2ScN@I_h$-C_{80}, and those distances are longer than the Gd−N distances in $Gd_3N@I_h$-C_{80}.

The positions of the metal ions within the idealized I_h-C_{80} cage show a propensity for the larger ions (Gd^{3+} or Tb^{3+}) to be situated over the centers of cage hexagons, as the drawings in Figures 2, 4, and 6 show for the major orientations of the metal ions. Additionally, note that the metal ions in $Tb_3N@I_h$-C_{80} and $Gd_3N@I_h$-C_{80} were also found to lie over hexagonal rings of the fullerene.[3,13] In contrast, the Sc^{3+} ion positions are more variable, with the Sc^{3+} ion usually lying near a 5:6 ring junction in the three new structures reported here.

The structures of the three new endohedrals considered here are compared with the structures of related endohedrals in Figures 8 and 9. Figure 8 shows views of the orientations of the M_3N units with respect to the plane of the adjacent metalloporphyrin for six different I_h-C_{80} endohedrals that possess planar M_3N units. For clarity, the locations of the C_{80} cages have been omitted in these drawings. However, the orientations of the portion of the cages closest to the metalloporphyrin plane are shown in Figure 9. There is a remarkable degree of consistency in Figure 8 in the orientations of the M_3N units, which lie roughly parallel to an N−M−N axis of the porphyrin and perpendicular to the porphyrin plane. Also notice the proclivity of the smaller Sc^{3+} ions to be near the porphyrin plane. Thus, $ErSc_2N@I_h$-C_{80}, $CeSc_2N@I_h$-C_{80}, $GdSc_2N@I_h$-C_{80}, and $TbSc_2N@I_h$-C_{80} all have the large ion located in the unique site furthest away from the porphyrin. In $Gd_2ScN@I_h$-C_{80}, the Gd_2ScN unit is again oriented so that the Sc^{3+} ion is near the porphyrin, one Gd^{3+} ion occupies the usual position furthest from the porphyrin, and the other Gd^{3+} ion is near the porphyrin plane, but not as near as the Sc^{3+} ion. There is also considerable consistency in the orientation of the C_{80} cage with respect to the porphyrin, as seen in Figure 9.

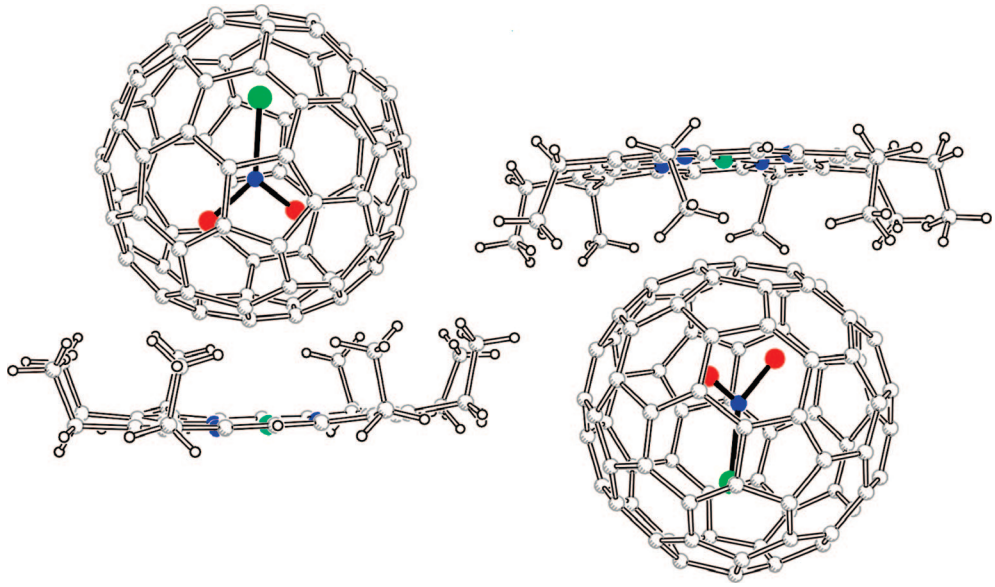

Figure 10. Drawing of two $GdSc_2N@I_h$-C_{80} molecules and two molecules of Ni^{II}(OEP) that pack with opposing dipoles about a center of symmetry in crystalline $GdSc_2N@I_h$-C_{80}·Ni^{II}(OEP)·$2C_6H_6$.

The consistency in the ordering of the M_3N units within the I_h-C_{80} cages in the porphyrin cocrystals is surprising given the general agreement from computational studies that examined the interactions between the metal ions and the fullerene cage.[33–35] These studies have all agreed that the barriers to reorientation of the M_3N units with the I_h cage are low. The presence of larger metal ions like Gd^{3+} or Tb^{3+} may alter the rotational barriers from those computed for $Sc_3N@I_h$-C_{80}. Additionally, at low temperatures, where the structures have been obtained crystallographically, the rotational barriers may be higher. Nevertheless, considering the high symmetry of the exterior of these endohedrals with their I_h cages, the degree of ordering of the internal portion seen in Figure 7 is quite remarkable and requires that these M_3N units order either during crystallization or upon cooling. Consideration has been given previously to the possibility that dipole forces may play a significant role in ordering the metal ion positions in the mixed-metal endohedral crystals.[22] Similar considerations may hold for the three cocrystals considered in the present study. While Ni^{II}(OEP) is nonpolar in solution, it acquires a small degree of polarity in the cocrystals by virtue of the positioning of the ethyl groups, which are all located on the same side of the porphyrin plane. The mixed-metal endohedrals have an intrinsic polarity due to the presence of two different metal ions inside. The three crystals considered here all are centrosymmetric. Consequently, there are local antiparallel alignments of the adjacent dipoles, as seen in Figure 10, which shows the centrosymmetric relationship between two $GdSc_2N@I_h$-C_{80}·Ni^{II}(OEP) units. While dipole–dipole interactions contribute to the ordering of the mixed-metal endohedrals shown in Figure 8, they will have a lesser impact in ordering a homometallic endohedral like the one found in $Sc_3N@I_h$-C_{80}·Co^{II}(OEP)·$CHCl_3$·$0.5C_6H_6$. Other factors to consider in determining the orientational ordering in these porphyrin cocrystals are the van der Waals forces, $\pi-\pi$ interactions, and electrostatic forces involved at the interface between the endohedral and the porphyrin.[36] In larger endohedrals, as seen in the series $Tb_3N@C_s$(51365)-C_{84}, $Tb_3N@D_3$-C_{86}, and $Tb_3N@D_3$(35)-C_{88}, steric factors appear to play a role.[3] In these cases, the planar Tb_3N units assume a variety of orientations. For example, in $Tb_3N@D_3$-C_{86}, that unit is nearly parallel to the plane of the porphyrin.

Experimental Section

Synthesis of Endohedral Fullerenes $GdSc_2N@I_h$-C_{80}, $Gd_2ScN@I_h$-C_{80}, and $TbSc_2N@I_h$-C_{80}. Samples of $GdSc_2N@I_h$-C_{80}, $Gd_2ScN@I_h$-C_{80}, and $TbSc_2N@I_h$-C_{80} were prepared using the electric-arc procedure described previously.[2] Packing material ratios were 2:6:1 (w/w) graphite/Gd_2O_3/Sc_2O_3 and 2:6:1 graphite/Tb_4O_7/Sc_2O_3. The collected soot was extracted with *o*-xylene (Aldrich), and the fullerene extract contained ~5% metallofullerene. Purifications of $GdSc_2N@I_h$-C_{80}, $Gd_2ScN@I_h$-C_{80}, and $TbSc_2N@I_h$-C_{80} samples were achieved with a two-stage procedure involving a crude separation using a PBB column (Phenomenex) to remove the more abundant, low-molecular-weight empty-cage fullerenes, followed by a final purification step with a BuckyPrep column (Phenomenex), as shown in Figure S.I.-1 in the Supporting Information, to resolve $GdSc_2N@I_h$-C_{80} from $Gd_2ScN@I_h$-C_{80}. Upon isolation, the purified samples were characterized by mass spectrometry prior to X-ray crystallography. Note that the separation protocol was repeated for the isolation of $TbSc_2N@I_h$-C_{80} from $Tb_2ScN@I_h$-C_{80}, and the HPLC trace was similar in peak shapes and elution order. All isolated $GdSc_2N@I_h$-C_{80}, $Gd_2ScN@I_h$-C_{80}, and $TbSc_2N@I_h$-C_{80} samples had purities of >95% by mass spectrometry.

Crystal Growth for Endohedrals. Cocrystals of Ni^{II}(OEP) with $GdSc_2N@I_h$-C_{80}, $TbSc_2N@I_h$-C_{80}, and $Gd_2ScN@I_h$-C_{80} were obtained by layering a red benzene solution of Ni^{II}(OEP) over a brown solution of ca. 0.25 mg of the endohedral in 0.5 mL benzene in a glass tube. Over a period of several weeks, the two solutions diffused together and black crystals formed.

(33) Campanera, J. M.; Bo, C.; Olmstead, M. M.; Balch, A. L.; Poblet, J. M. *J. Phys. Chem. A* **2002**, *106*, 12356.
(34) Gan, L. H.; Yuan, R. *ChemPhysChem* **2006**, *7*, 1306.
(35) Liu, D.; Hagelberg, F.; Park, S. S. *Chem. Phys.* **2006**, *330*, 380.
(36) Hunter, C. A.; Sanders, J. K. M. *J. Am. Chem. Soc.* **1990**, *112*, 5525.

X-ray Crystallography and Data Collection. The crystals were removed from the glass tubes in which they were grown together with a small amount of mother liquor and immediately coated with hydrocarbon oil on the microscope slide. A suitable crystal of $Gd_2ScN@I_h\text{-}C_{80}\cdot Ni^{II}(OEP)\cdot 2C_6H_6$ was mounted on a glass fiber with silicone grease and placed in the cold dinitrogen stream of a Bruker ApexII diffractometer with graphite-monochromated Mo Kα radiation at 90(2) K. Data for crystals of $GdSc_2N@I_h\text{-}C_{80}\cdot Ni^{II}(OEP)\cdot 2C_6H_6$ and $TbSc_2N@I_h\text{-}C_{80}\cdot Ni^{II}(OEP)\cdot 2C_6H_6$ were obtained at BL9-1 at the Stanford Synchrotron Radiation Laboratory (SSRL) with the use of a silicon monochromator with 0.751 00 Å synchrotron radiation at 100(2) K. Crystal data are given in Table 1. The structures were solved by direct methods and refined using all data (based on F^2) using the software of *SHELXTL5.1*. The numbering scheme used for the three structures reported here uses a systematic array that becomes discontinuous between C40 and C41. This is the same system as that used in our other studies of $I_h\text{-}C_{80}$ endohedrals and differs from the IUPAC scheme, which is discontinuous between C75 and C76. $Gd_2ScN@I_h\text{-}C_{80}\cdot Ni^{II}(OEP)\cdot 2C_6H_6$, a semiempirical method utilizing equivalents, was employed to correct for absorption.[37] Hydrogen atoms were located in a difference map, added geometrically, and refined with a riding model.

Acknowledgment. We thank the National Science Foundation (Grants CHE-0716843 and CHE-0413857 to A.L.B. and Grant CHE-0547988 to S.S.) for support. The SSRL is funded by the U.S. Department of Energy and the National Institutes of Health. We thank Dr. Paul Ellis for experimental assistance.

Supporting Information Available: Figure S.I.-1, a packing diagram for $Gd_2ScN@I_h\text{-}C_{80}\cdot Ni^{II}(OEP)\cdot 2C_6H_6$, and X-ray crystallographic files in CIF format for $GdSc_2N@I_h\text{-}C_{80}\cdot Ni^{II}(OEP)\cdot 2C_6H_6$, $Gd_2ScN@I_h\text{-}C_{80}\cdot Ni^{II}(OEP)\cdot 2C_6H_6$, and $TbSc_2N@I_h\text{-}C_{80}\cdot Ni^{II}(OEP)\cdot 2C_6H_6$. This material is available free of charge via the Internet at http://pubs.acs.org.

IC701824Q

(37) *SADABS 2.10* based on a method of R. H. Blessing: Sheldrick, G. M. *Acta Crystallogr., Sect. A* **1995**, *A51*, 33.